Figure 5-14 graphically shows the average output force for each type of bent-beam electrothermal actuator, along with one standard deviation from the calculated average. These averages are based on the two force data points (for the 100 μ m and 200 μ m cantilever beams only) provided in Table 5-2. The standard deviations provide some confidence that the force tests produced valid results for each type of actuator, except the 400 μ m \times 8 straight arm actuator. This actuator has an extremely large standard deviation due to the large difference between the two maximum beam deflections (100 μ m and 200 μ m beams only). This suggests the existence of a random error in one, or both, of these measurements. To determine the true output force for this actuator would require additional testing.

Another possible error source is the cantilever beam width used for calculating the output force. The value of 7 μ m for the beam width was determined from measurements taken in the SEM, however this method produced an uncertainty of \pm 0.25 μ m. Thus, the width variable in Equation (4.7) can range from 6.75 μ m to 7.25 μ m. Since the calculated force is dependent on the cube of the width, any small variations in this

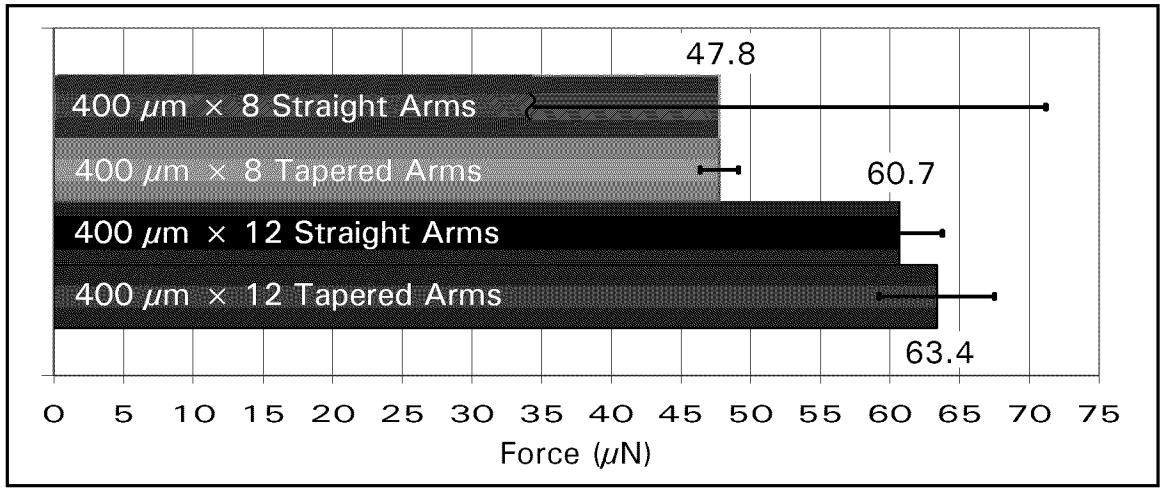


Figure 5-14. Average output force for each type of bent-beam electrothermal actuator, along with one standard deviation from the calculated averages based on the two force data points (for the 100 μm and 200 μm cantilever beams) provided in Table 5-2.

measurement may produce a significant error. For example, the widths of 6.75 μ m and 7.25 μ m correspond to force measurements of 43.7 μ N and 54.1 μ N, respectively, when using the data for the 400 μ m \times 8 tapered arm actuator. In addition, note the uncertainty in the beam lengths is not as significant, since even an uncertainty of \pm 2 μ m does not have a large effect on the calculated forces. For example, considering a 200 μ m \pm 2 μ m range in beam lengths, the corresponding change in calculated force would be 50.2 μ N and 47.3 μ N, respectively.

Nevertheless, Figure 5-14 does clearly show a higher output force being produced by the 12 armed actuators than the 8 armed actuators, as suggested by the bent-beam actuator theory discussed in Section 4.3.3. Moreover, the micro-newton forces produced by the bent-beam actuators are significantly higher than the required nano-newton forces shown in Table 4-3. To conclude, the bent-beam actuators designed for the interrupter mechanism should have plenty of force to separate the interrupter plates and provide an aperture for the flyer material to pass through.

5.3 Interrupter Mechanism Tests

The final test in this research effort was to determine the operating characteristics of the fabricated MEMS S&A interrupter device, which was first presented in Section 4.2 and shown in Figure 4-6. Recall that this device has two main functions: 1) to impede the path of the flyer material in a solid-state slapper, thus preventing inadvertent initiation of an explosive train, and 2) to create an unimpeded path for flyer material so it can impact the HE pellet and initiate an explosive train. Assuming the first function is satisfied by the initial "closed" position of the four interrupter plates (shown in Figure 4-18); only the second function needs to be demonstrated. Since the interrupter plates are attached to the

end of the bent-beam electrothermal actuators, an experiment was designed to simultaneously power the individual actuators, which will cause the interrupter plates to move linearly outward, thus creating an open area for the flyer material to pass through.

The design layouts for the specific interrupter mechanisms tested are shown in Appendix C as Die #11 (Interrupter #1), Die #14 (Interrupter #2), and Die #15 (Interrupter #3). In addition, Table 4-2 shows the type of bent-beam actuators incorporated into each of these three interrupter mechanisms. Prior to testing each fabricated die, the release procedures, outlined in Appendix A, were accomplished. In addition, the same equipment described previously for the stand-alone actuator tests was again used to perform the following experiments and capture the results. Specifically, this equipment was the Micromanipulator probe station, the Agilent DC power supply and digital multimeter, the Optronics microscope camera, and the ATI video capturing software.

In order to supply power to all the actuators at the same time, five microprobes were used to facilitate the electrical connections. The initial intention was to power the device using only two microprobes and the fabricated Metal and Poly0 wires shown in Figure 4-6. However, upon initial testing it was determined that the much higher resistance (by two orders of magnitude) of the Poly0 wires, as compared to the Metal wires, made this approach impossible to implement. Therefore, it was concluded that the best alternative approach was to connect five microprobes to the actuators of the interrupter mechanism as shown in Figure 5-15. Figure 5-15(a) shows a simplified circuit model for the interrupter mechanism and Figure 5-15(b) shows an actual image of an interrupter mechanism with five microprobes connected to the four 400 µm × 12

straight arm actuators. Since the Metal wires offered a resistance of approximately 2 - 10 Ω , they worked well for supplying the input voltage to each actuator.

Furthermore, the four parallel resisters shown in Figure 5-15(a) can be reduced into a single resistive value for the complete interrupter mechanism. Figure 5-16 shows

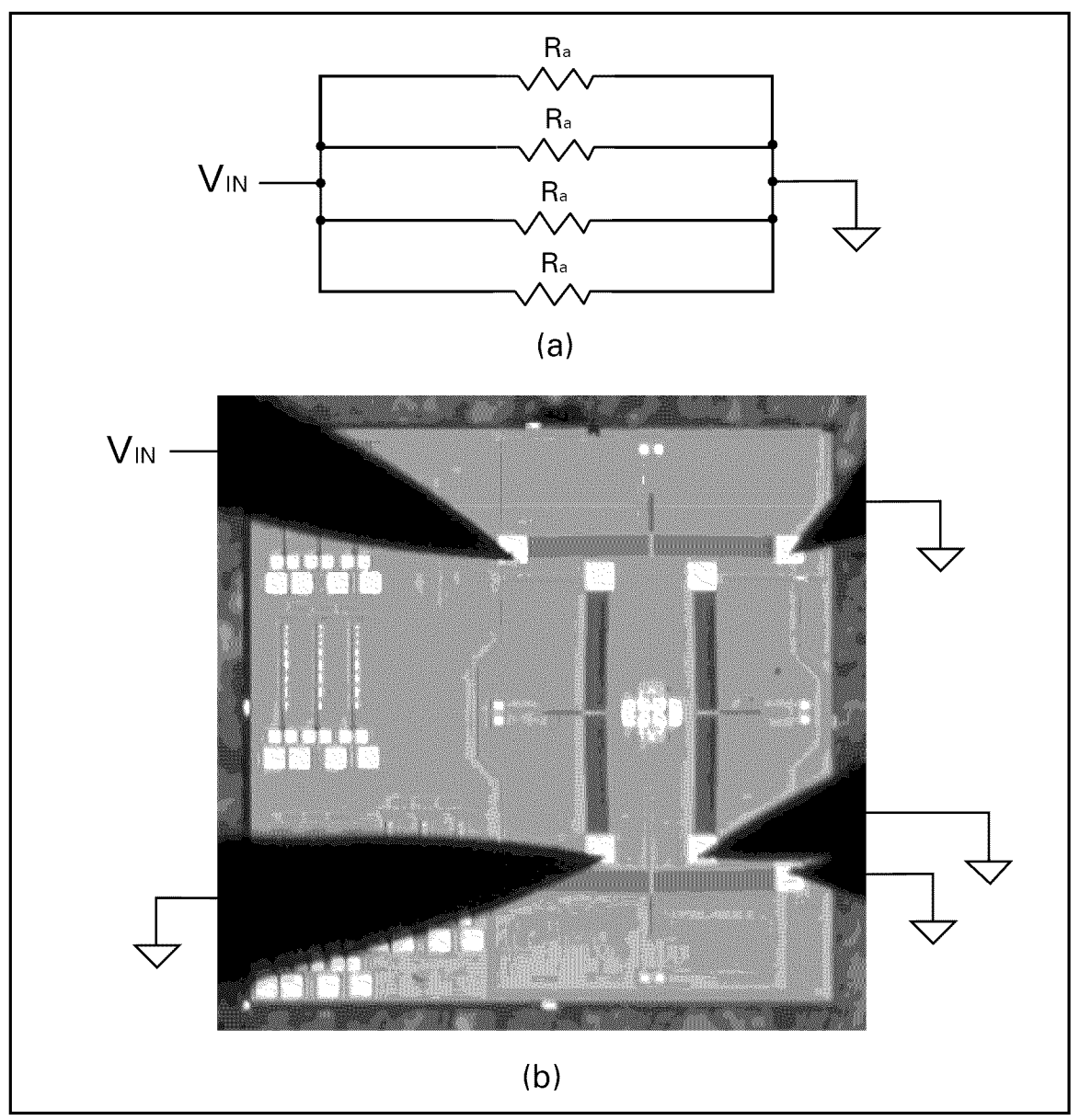


Figure 5-15. (a) Equivalent circuit model for the interrupter mechanism, where R_a is given by the actuators' resistance values shown in Figure 4-6. (b) Image of actual interrupter mechanism (just prior to activation) showing how the electrical circuit was connected. Note: this image is from Die #14, which uses four 400 μ m \times 12 straight arm actuators.

the resistance values for all three of the fabricated interrupter mechanisms, along with the standard deviation based on measurements of at least three separate devices. These results are similar to those observed with the individual actuators. For instance, the interrupter mechanisms with 12 arm actuators have a lower resistance than those with 8 arms, and the interrupters with tapered arm actuators produce a lower resistance over the ones with straight arms.

Based on these resistance results, it is expected that the interrupter mechanisms fabricated with the 400 $\mu m \times 8$ straight arm actuators will have the lowest operating power. Figure 5-17 shows the measured power requirements for each interrupter mechanism. As can be observed, the interrupter with the 400 $\mu m \times 8$ straight arm actuators does indeed have a lower operating power for a given applied voltage. In

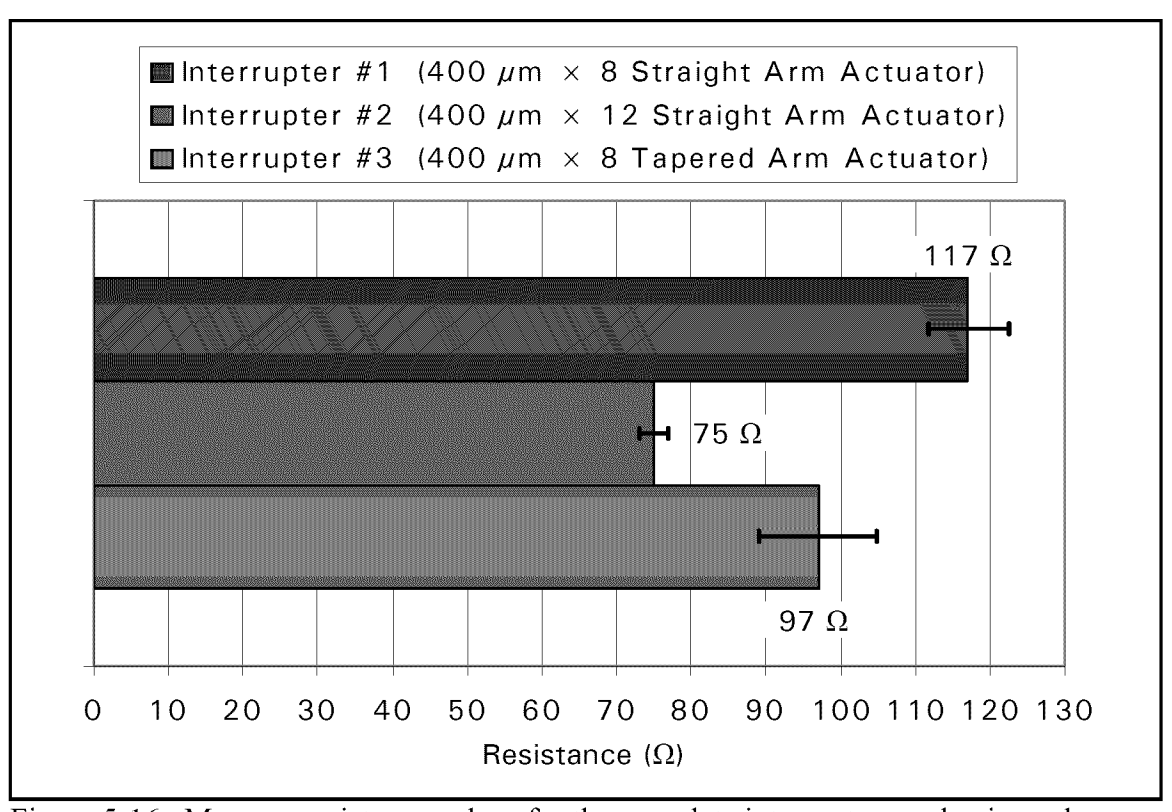


Figure 5-16. Measure resistance values for the complete interrupter mechanism, along with the standard deviation based on measurements of at least three separate devices.

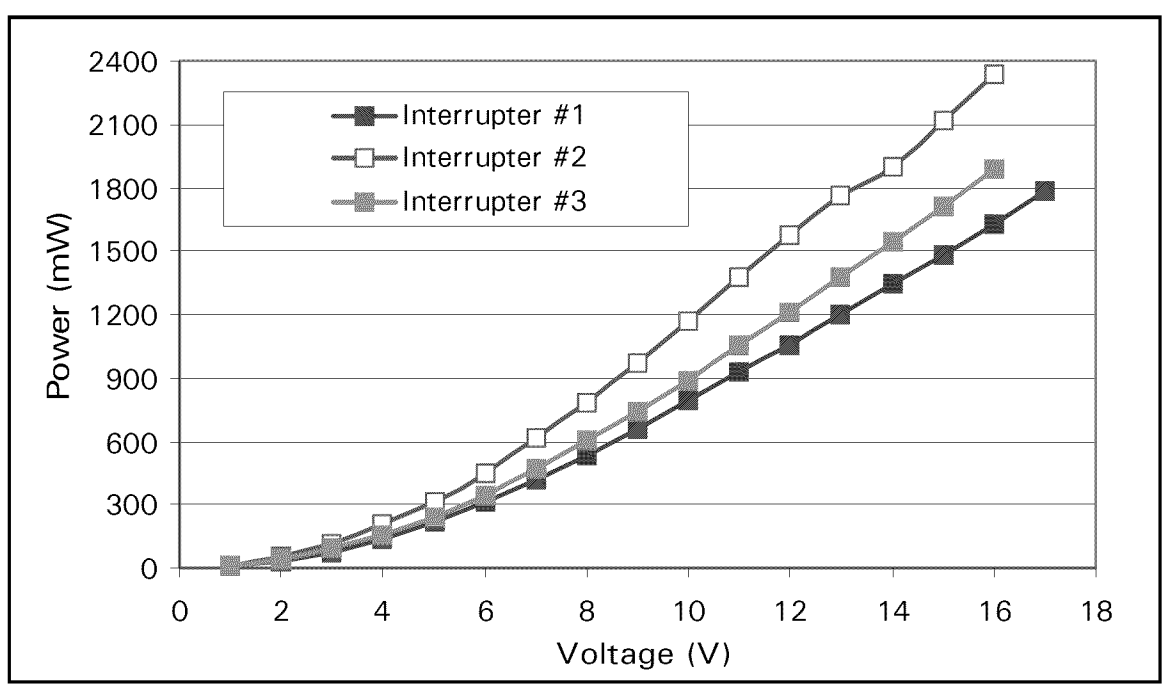


Figure 5-17. Input power as a function of the applied voltage for each interrupter mechanism. Consistent with the results seen in Section 5.2.1, the interrupter mechanism with the 400 μ m \times 8 straight armed actuators has the lowest power requirements.

addition, Figure 5-17 shows that the maximum operating voltage of these interrupter mechanisms is approximately 16-17 V. Higher applied voltages tended to result in at least one of the actuators suffering a catastrophic thermal failure.

Finally, to show functionality of the interrupter mechanism, the DC power supply was used to step the input voltage from 0 V to 15 V. This maximum voltage was selected to prevent thermal failure of any actuator and to ensure that repeatable device operation could be shown. Still images were captured for each voltage step using the video capturing equipment and the area of the aperture was estimated by comparing the distance between dimples and etch holes fabricated on the interrupter plates. In addition, deflection was measured using the Poly0 measuring scales fabricated alongside the latching arm extension, and these measurements were used to confirm the opened area estimations made by observing features on the interrupter plates.

The objective for these interrupter mechanism experiments was to demonstrate simultaneous actuation of the four independent interrupter plates, thus creating an opened area in the otherwise closed interrupter mechanism. Figure 5-18 shows an example of this objective being met for Interrupter #3 at four different voltages ranging from 0 V to 15 V. Clearly, the still images of this MEMS interrupter mechanism successfully demonstrates the four interrupter plates independently moving linearly outward to produce an aperture. By comparing the distances between features on the interrupter plates, the dimensions of the maximum opened area can be estimated to be approximately $32~\mu m \times 32~\mu m$. This implies that the maximum deflection attained by the four parallel bent-beam actuators is only 15 μm , which is about 88% of the maximum deflection (17 μm) observed in Figure 5-9. Therefore, an aperture area of approximately $1024~\mu m^2$ was produced, as opposed to the $1300~\mu m^2$ that would have resulted for a 17 μm actuator deflection, as suggested in Section 5.2.1.

This same experiment was performed repeatedly with Interrupters #1, #2, and #3, with similar results being observed for all three interrupter mechanisms, i.e., no perceivable differences in performance were discerned. Therefore, the only comparisons that could be made between the three interrupter mechanisms are based on the individual actuator performance discussed above.

Figure 5-19 and Figure 5-20 show the operation of Interrupter #1 (20X magnification) and Interrupter #2 (10X magnification), respectively. Both images show the interrupter mechanism at 0 V and at 15 V. Observe the expansion of the bent-beam actuator arms, which causes deflection and separation of the interrupter plates, in Figure 5-19(b) and Figure 5-20(b), respectively.

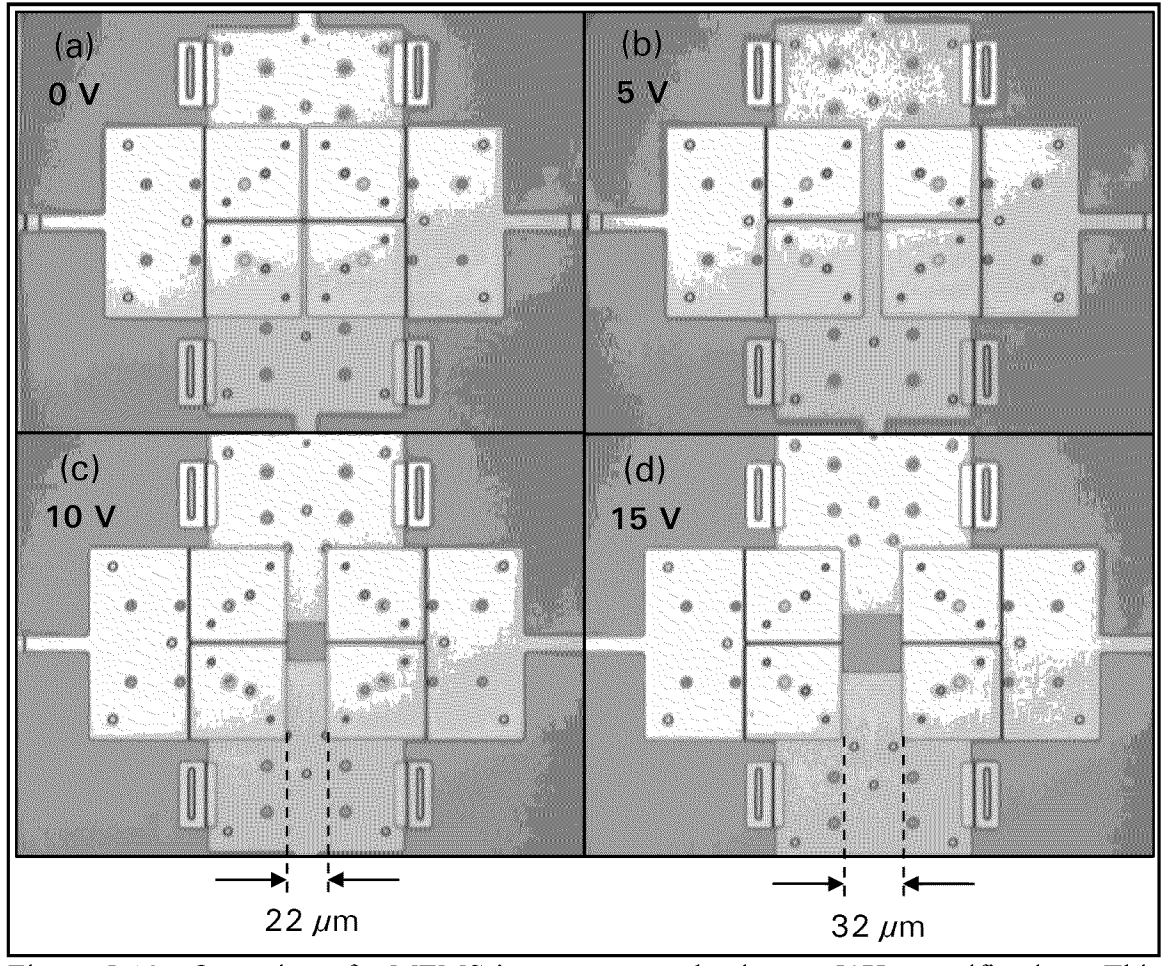


Figure 5-18. Operation of a MEMS interrupter mechanism at 50X magnification. This sequence of images shows Interrupter #3 at: (a) 0 V, (b) 5 V, (c) 10 V, and (b) 15 V.

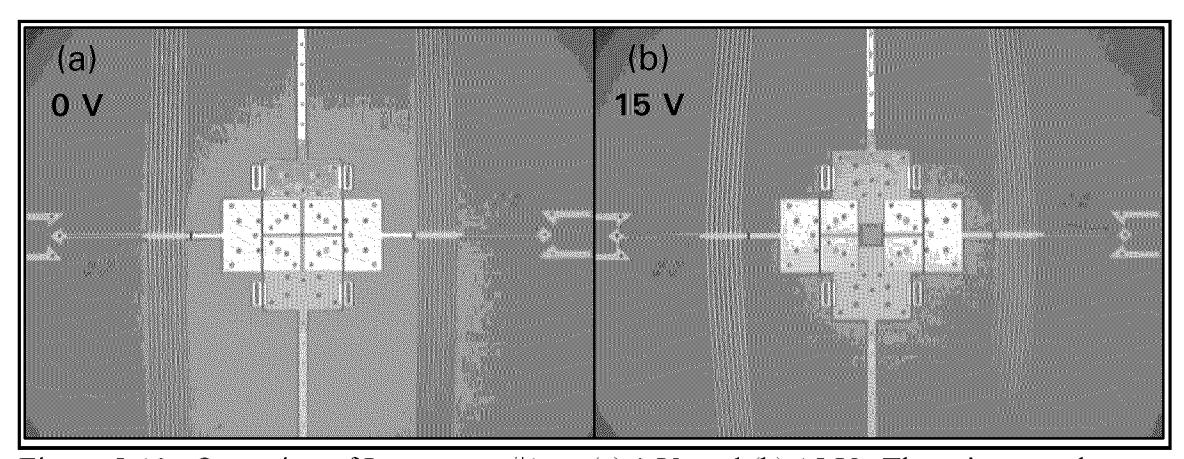


Figure 5-19. Operation of Interrupter #1 at: (a) 0 V, and (b) 15 V. These images show center of interrupter mechanism at 20X magnification. Note: the expansion of the bent-beam actuator arms is visible in (b).

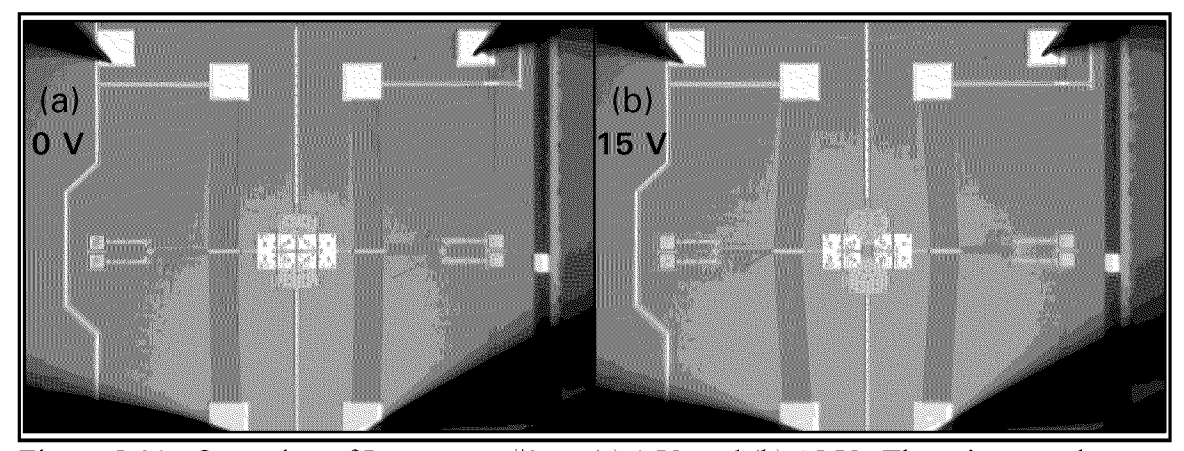


Figure 5-20. Operation of Interrupter #2 at: (a) 0 V, and (b) 15 V. These images show center of interrupter mechanism at 10X magnification. Again, note the expansion of the bent-beam actuator arms in (b).

An examination of the latching arm extension of the interrupter mechanism, and the Poly0 measuring scale, revealed that the actuators were limited to 15 µm deflection by the inability of the actuators to force open the fixed component of the latching mechanism. Figure 5-21 shows an actuator at this maximum deflection point. Notice the measuring scale indicates a deflection of approximately 15 µm, which confirms the estimated deflection that was based on the features of the opened interrupter plates.

A quick analysis of the fixed latching component, using Equation (4.7), shows that approximately 900 μ N of force would be required to move one of the 11- μ m wide by 100- μ m long beams the 5 μ m distance necessary to enable latching. This required force is one order of magnitude greater than the lateral output force produced by the bent-beam actuators, as shown in Table 5-2. Therefore, in order to produce the necessary 5 μ m deflection of the fixed latching components, the beam widths need to be decreased to approximately 3 - 4 μ m, which would result in a required actuator force of approximately 18 - 43 μ N, respectively. Clearly, this range of required output forces is within the

capabilities of the actuators tested in this research effort. The design layout shown in

Figure 5-22 indicates the designed dimensions for the latching mechanism.

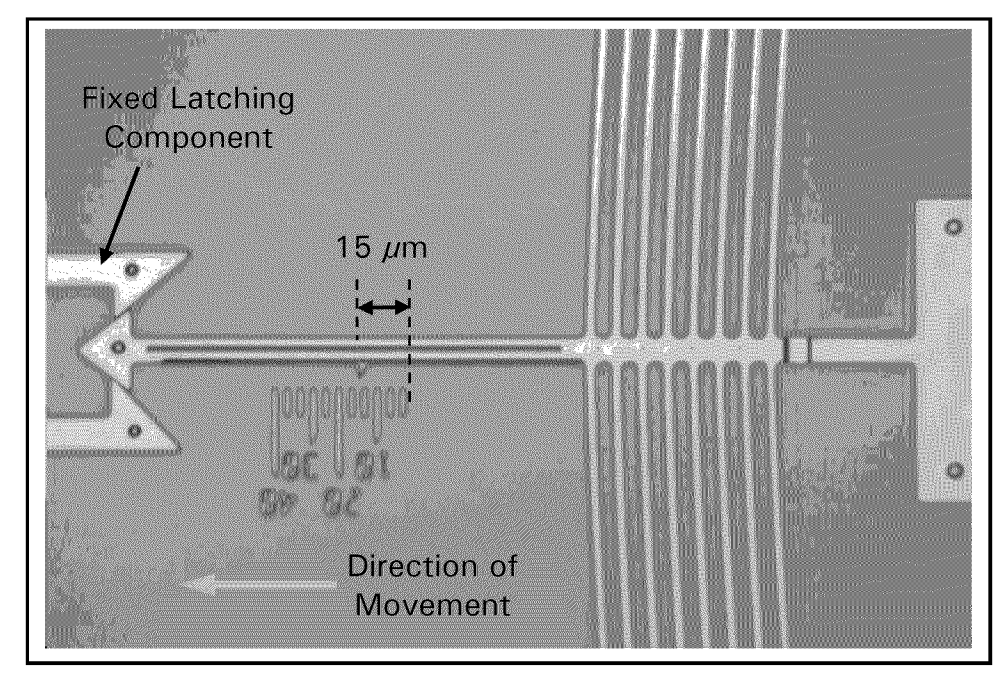


Figure 5-21. Maximum actuator deflection shown at 50X magnification. The inability of the actuator to move the fixed latching components limits the maximum deflection of each actuator to approximately $15~\mu m$.

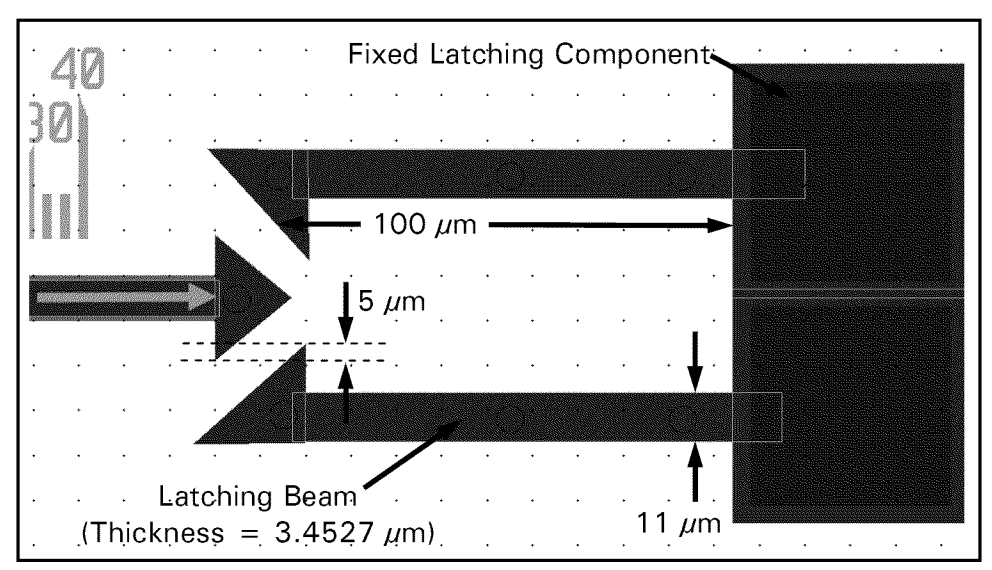


Figure 5-22. Design layout of latching components for interrupter mechanism. The latching beams require a force of approximately 900 μ N to produce the 5 μ m deflection required for latching to occur. This force value is based on the length and width of the designed beam. Note: the latching beam thickness is a result of the stacked Poly1 + Poly design.

5.4 Summary

This chapter presented the test results performed on the fabricated interrupter mechanism and its individual components, in an effort to determine the overall effectiveness of the conceptual MEMS interrupter design. The tests on the PolyMUMPs fabrication process determined that the minimum separation distance between the two interrupter plates should be no closer than 2 μ m, thus ensuring that they are not fabricated as one structure. In addition, the performance characteristics of the four individual bent-beam actuators showed that the 400 μ m \times 8 straight arm actuator performed the best, in terms of its relatively large deflection and low operating power. Even though this actuator produced 20% less force than the 12 armed actuators, the lower operating power makes the 400 μ m \times 8 straight arm actuator a better choice over the other tested actuators. Finally, the operation of the complete interrupter mechanism demonstrated the feasibility of using this device to create an aperture for the flyer material, in a solid-state slapper detonator, to pass through on its way to initiating a HE pellet.

Bibliography

- [1] Koester, David and others. *PolyMUMPs Design Handbook (Revision 11.0)*. MEMSCAP, 2005. August 2005. http://www.memsrus.com/documents/PolyMUMPs.DR.v11.pdf.
- [2] Sinclair, Michael J. and Kerwin Wang. "Thermal Actuator Improvements: Tapering and Folding," *Proceedings of the SPIE The International Society for Optical Engineering*. Volume 5116: 237-251 (April 2003).
- [3] "PolyMUMPs.rundata.xls." *PolyMUMPs Run Data*. http://www.memsrus.com/nc-pmumps.refs.html.
- [4] Jaeger, Richard C. *Introduction to Microelectronic Fabrication* (2nd Edition). New Jersey: Prentice Hall, 2002.
- [5] Sharpe Jr., W. N., K. Jackson, G. Coles, and D. A. LaVan. "Young's Modulus and Fracture Strength of Three Polysilicons," *Proceedings of Materials Science of Microelectromechanical Systems (MEMS) Devices III.* Volume 657: 551-556. Materials Research Society, 2001.

6. Conclusions and Recommendations

The objective of this research effort was to investigate a MEMS-based solution to a problem that has been facing the munitions community in recent years – the aging stockpile of weapon system components (e.g., fuzes and S&A devices). The aging problem is compounded by the decreasing number of weapon component manufacturers over the last 15 years [1]–[3]. Therefore, a practical replenishment program, that considers both old and new weapon systems, is desirable. Since MEMS devices have inherent benefits over their macro-scale counterparts (e.g., significantly lower costs per unit due to their large fabrication volumes), they offer an obvious area to explore for potential exploitation.

The approach taken in this research was to design, fabricate, and test a conceptual interrupter mechanism to determine the feasibility of operating a MEMS device for this purpose. For instance, the designed S&A interrupter device had to have a normally closed configuration (safe), and be capable of forming an opened area (armed) upon activation. This type of device was successfully demonstrated, as described in Chapter 5, and conclusions based on the observed results will be briefly discussed in this chapter. In addition, recommendations for future work will also be discussed.

6.1 Conclusions and Recommendations Based on Experimental Work

Several different aspects of the interrupter mechanism were tested in an effort to better characterize the operation of the complete device. The fabrication process was investigated to understand its limits and determine if any design parameters could be optimized. The stand-alone actuators were tested to provide a baseline for their performance in order to better characterize the performance of the fabricated interrupter mechanism. Finally, the complete interrupter mechanism was tested to ensure device operation, in addition to collecting performance data.

6.1.1 Fabrication Process

The interrupter mechanisms designed in this research effort were fabricated exclusively in the PolyMUMPs fabrication process. To investigate the limitations of this process, several test structures were fabricated to get an understanding of the process constraints that will effect any future modifications of the existing interrupter mechanism.

First, width test structures (shown in Figure 5-1) were used to investigate the minimum design width for the bent-beam actuator arms, to determine if a narrower arm could be fabricated that could possibly increase deflection for future actuator designs. If more deflection could be produced, then a larger aperture could be created. The results of these tests showed that beams fabricated in the individual polysilicon layers (Poly1 and Poly2) could be fabricated to a 2 μ m width, however, these test structures did not consider a 3.5- μ m thick (Poly1 + Poly2) beam, which the PolyMUMPs design rules suggest should have a minimum line width of 3.5 μ m [4]. Nevertheless, the width of the actuators' arms fabricated in this thesis was 3 μ m, and satisfactory performance was observed, however, this does not imply anything about the performance of these actuators over time, nor does it imply that the fabrication process would yield the same results over many runs. A recommendation for future work would be to determine the performance characteristics of bent-beam actuators with arms that are narrower than 3 μ m. Figure 6-1 shows an image of a bent-beam electrothermal actuator, with 2.5- μ m wide × 3.5- μ m

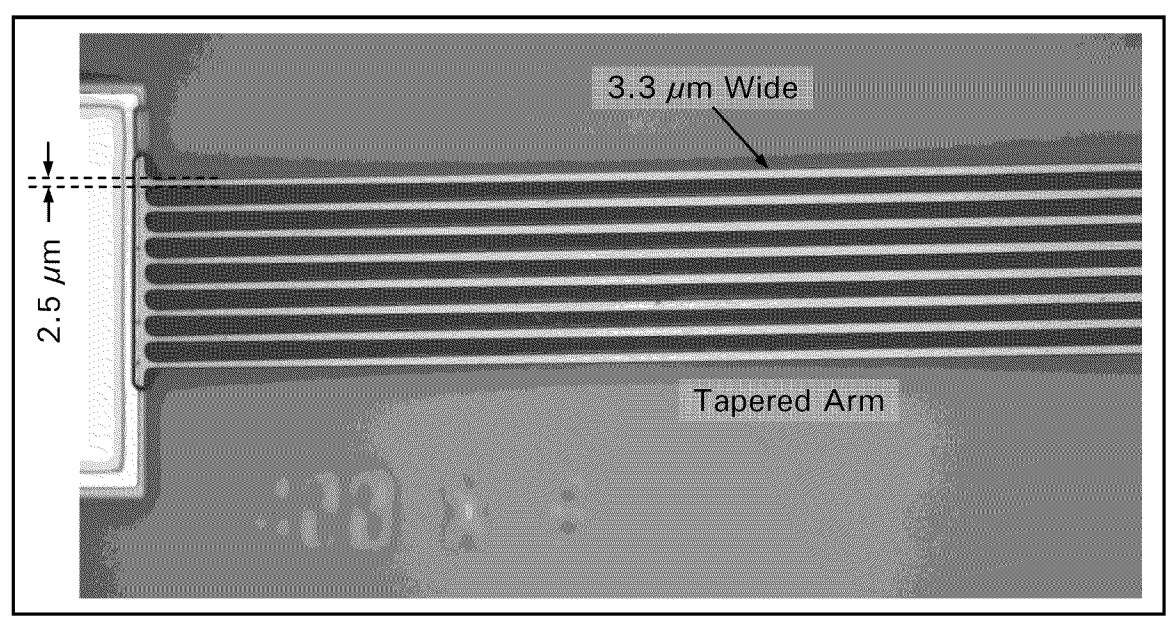


Figure 6-1. Image of a 400 μ m \times 8 tapered arm electrothermal actuator, fabricated in run #69, shown at 100X magnification. This figure shows that 2.5- μ m wide \times 3.5- μ m thick arms could be fabricated in the PolyMUMPs process.

thick arms at the anchor points, that was fabricated in run #69. These arms appear to be satisfactorily fabricated; however, its operating performance was never examined due to time constraints.

Next, spacing test structures (shown in Figure 5-2 and Figure 5-3) were used to investigate the minimum spacing between two structures of the same material layer. This spacing defines the minimal opened area of the "closed" interrupter, which could be reduced if the spacing could be minimized. The results of the spacing test structures confirm that the designed 2 μ m minimum spacing between the similar materials was a suitable choice for the interrupter mechanism fabricated for this research, and that a spacing of 1 μ m should be avoided. Therefore, it appears that the minimum *designed* aperture area is 4 μ m². However, Figure 6-2 shows an image of the center of a fabricated interrupter mechanism, which indicates that the fabricated spacing is a little larger (by 0.5 μ m) than the designed spacing. This resulted in a minimum *fabricated* aperture area of

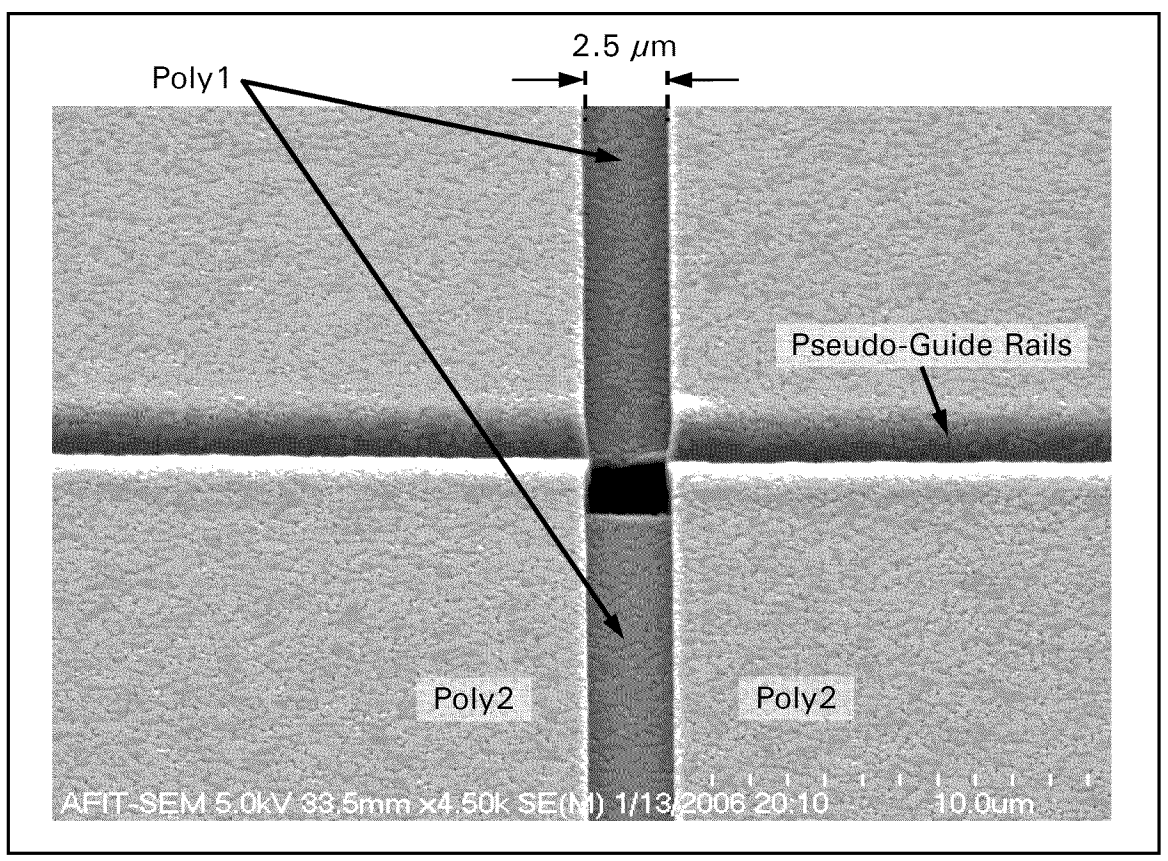


Figure 6-2. SEM image showing interrupter mechanism. The fabricated spacing between the two structures of the same material layer was measured to 2.5 μ m (Designed spacing was 2 μ m.) This produced a "closed" aperture area of 6.25 μ m² (Designed to be 4 μ m².) Note: the pseudo-guide rails that were formed on the Poly2 layer as a result of the spacing between the two Poly1 layers and the conformality of the fabrication process.

6.25 μm^2 . Also, note from Figure 6-2, that pseudo-guide rails are formed on the Poly2 layer as a result of the spacing between the two Poly1 layers and the conformality of the fabrication process. It was concluded that these rails may actually help to ensure smooth operation of the interrupter mechanism as power is applied. A recommendation for future work would be to determine if the spacing could be reduced further by designing spacing test structures that have gaps between 1 - 2 μ m (e.g., 1.75 μ m, 1.5 μ m, or 1.25 μ m). This could potentially decrease the initial designed aperture area from 4 μ m² (at 2 μ m spacing) to 3.06 μ m², 2.25 μ m², or 1.56 μ m², respectively.

The last process consideration that should be discussed is how significant a factor the thickness of the interrupter plates (Poly1 - 2 µm and Poly2 - 1.5 µm), play in preventing the energy of the flyer material from passing through the closed interrupter. The approach taken here was to increase the blocking strength of the interrupter by arranging the four interrupter plates in an overlapping pattern. However, the effectiveness of this approach was never examined. Therefore, future work in this area could include determining if the overlapping interrupter plates could absorb the energy imparted on the flyer material by the slapper detonator. As a further recommendation, if it is determined that the two overlapping polysilicon interrupter plates are inadequate, an alternative fabrication process, such as MetalMUMPs[™], could be selected. MetalMUMPs is another process offered by the MUMPs® foundry that uses a 20-μm thick, electroplated nickel layer as the primary structural material [5]. In addition to being a much thicker layer than polysilicon, nickel has a larger density (9.04 g/cm³) and a higher Young's modulus (210 GPa) than polysilicon (2.33 g/cm³ and 158 GPa, respectively) [6], [7]; and thus would provide for a stronger interruption barrier.

6.1.2 Stand-Alone Actuators

Four types of stand-alone bent-beam electrothermal actuators (the three listed in Table 4-2 plus the 400 μ m \times 12 *tapered* arm actuator used to provide completeness) were designed to assist in characterizing the complete interrupter mechanism. The only varied parameters were the number of arm pairs (8 or 12) and whether the arms were straight or tapered. Tests were performed to determine the actuator deflection as a function of input power, as well as the output force generated by each actuator type.

First, data was collected from 27 stand-alone bent-beam electrothermal actuators in order to characterize the deflection and power relationship for each of the four types of actuators. The results showed that the best performance, in terms of greatest deflection for the least amount of input power, was from the 400 μ m \times 8 straight arm actuator. These results were consistent with what was expected based on the measured resistance of each actuator, which showed that the 400 μ m \times 8 straight arm actuator had the largest resistance of all the other actuators. In this case, the larger resistance caused a reduced power requirement for a given deflection, since the higher resistance resulted in less current being needed to thermally expand the arms and cause deflection.

Next, data was collected from 36 stand-alone bent-beam actuators that were fabricated adjacent to cantilever beams of varying lengths to determine the output force being generated by each actuator type. By measuring the maximum beam deflection produced by the actuators, the output force could be calculated using Equation (4.7). Theoretically, for a given actuator, three different maximum beam deflections should be observed, with the output force calculations producing the same results. However, an anomaly existed for the results produced by the 300 µm cantilever beam. It was determined that since the theoretical maximum deflection for the 300 µm beam was beyond the deflection capability of the actuator, the results obtained from this beam were invalid. In contrast, the results from the 100 µm and 200 µm cantilever beam measurements, agreed to within less than 10%, for three out of four of the actuator types tested. As expected from the bent-beam actuator theory discussed in Section 4.3.3, the greatest force was produced by the actuator with the greater number of arm pairs (i.e., the actuators with 12 arms produced greater output force than those with 8 arms).

Recommendations for future work would be to determine the deflection and force characteristics of the bent-beam electrothermal actuators fabricated in run #69. These actuators are similar to the ones fabricated for this thesis, except that the straight arms have a 2.5 µm width, and the tapered arms have been adjusted accordingly to maintain the 1.32 C/D ratios, as discussed in Section 4.4.1.

6.1.3 Interrupter Mechanism

The final test was to demonstrate the operation of the complete MEMS interrupter mechanism, to determine if the device was capable of being actuated from the normally closed configuration to an opened configuration. For each of the three interrupter mechanisms tested, successful lateral motion of the interrupter plates created an aperture that was repeatedly observed. In addition, it is clear from Figure 5-18, Figure 5-19, and Figure 5-20, that simultaneous operation of all four actuators in each interrupter mechanism was achieved. The opened area created by the interrupter plates was determined from the captured still images to be a little less than expected (1024 µm² as opposed to 1300 µm²) since the actuators were limited to only 15 µm of deflection by the latching mechanism. After examining the stand-alone deflection data, it was noticed that the power increase needed to produce a deflection greater than 17 µm, usually resulted in thermal failure of at least one arm of the actuator. Therefore, it is reasonable to conclude that the actual operation of the interrupter mechanism should not attempt to obtain the maximum deflection of the individual actuator, but should be operated at a reduced power to ensure an adequate margin exists to account for uncertainties in the complete system.

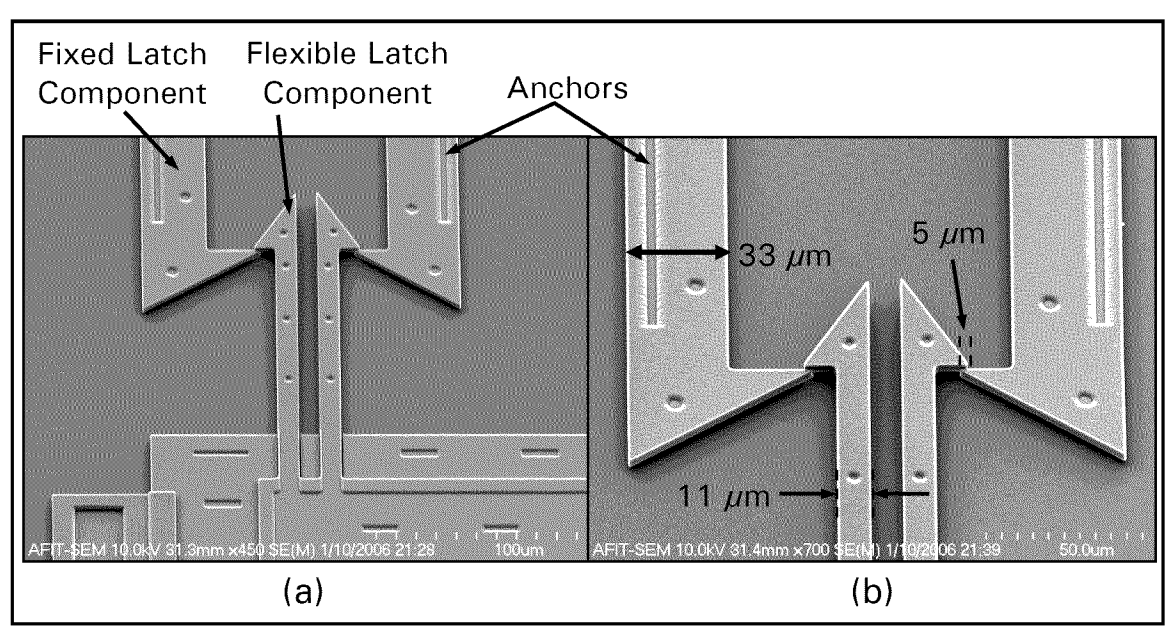


Figure 6-3. (a) Alternative latching mechanism that was fabricated in PolyMUMPs run #68 using both Poly and Poly2. This latch was demonstrated by using a microprobe to push the structure until latching occurred. (b) Magnified view of (a) showing the two latching components are "latched" at only a 5 µm portion of the locking mechanism. However, the validity of the latching mechanism was clearly demonstrated, and better results could be obtained by optimizing this design.

A recommendation for future work is to design a latching mechanism that is capable of locking the interrupter plates in the opened position. An alternative latching mechanism that was fabricated in PolyMUMPs run #68 is shown in Figure 6-3. Based on preliminary testing that was performed, it was concluded that this mechanism was more successful than the latches used in the interrupter mechanisms. However, it can be observed in Figure 6-3(b) that the "latching" occurs for only a very small portion (5 μm) of the locking mechanism, and thus further modifications and testing would be necessary to obtain better results. Also, note that the latching seen here was the result of a microprobe being used to push the structure into its latched position.

Finally, there were no issues that prevented the actuators from separating the interrupter plates repeatedly for each interrupter mechanism tested. On the other hand,

there was some initial binding on the interrupter plates due to an inadvertent design error. For each interrupter tested, the initial binding was eliminated after a one-time voltage (6-7 V) was applied to the device. Figure 6-4(a) shows several fabricated features (each designed to a diameter of 6 µm) on the surface of the interrupter plates that could have contributed to the binding. However, it was concluded based on these images that the most likely cause for the binding was the result of the Poly2 material over a Poly1 etch hole, as shown in Figure 6-4(b). A recommendation to eliminate this from occurring is to either, line up the Poly1 and Poly2 etch holes, or completely avoid fabricating Poly1 etch holes where it is desirable for Poly2 to cover Poly1.

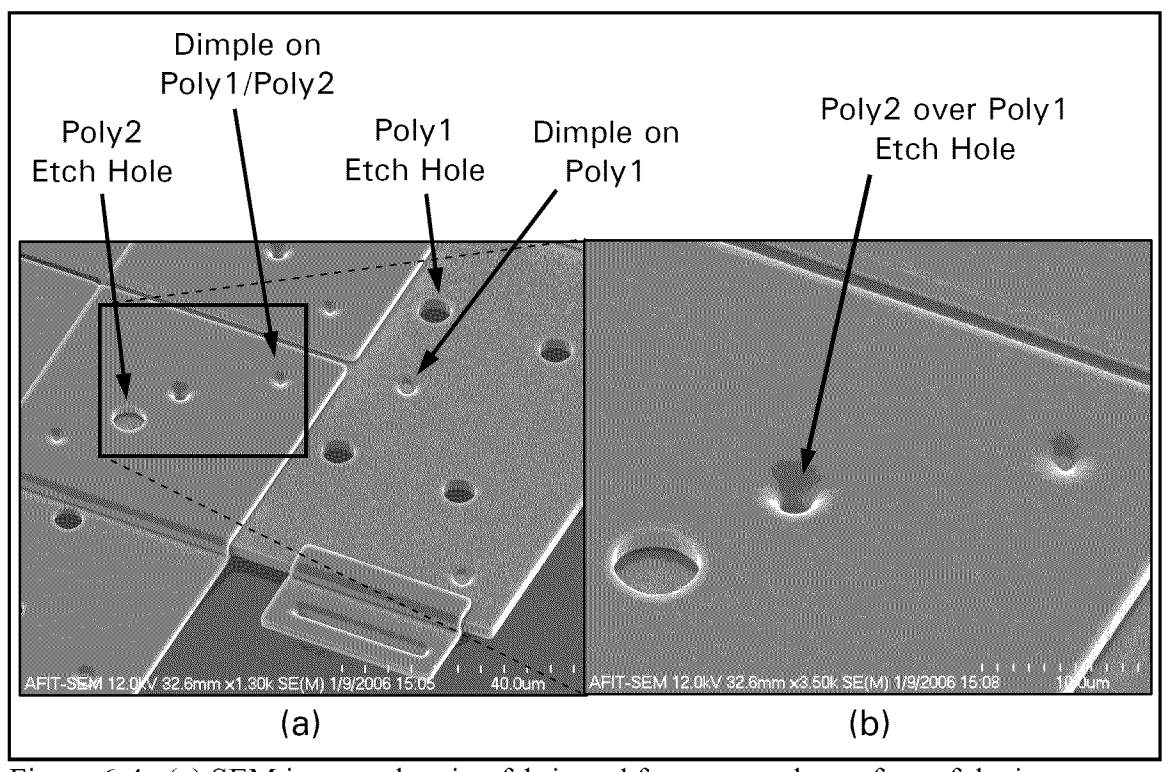


Figure 6-4. (a) SEM images showing fabricated features on the surface of the interrupter plates. All of the following features were designed to a diameter of 6 µm: dimples shown on both Poly1 and Poly2, Poly1 etch holes, Poly2 etch holes, and an inadvertent error – Poly1 etch hole under a Poly2 layer.

6.2 Recommendations for Future Work

Since the interrupter mechanism designed in this research effort is a conceptual device, many opportunities exist for this device to be optimized. In addition, there are other MEMS methods that can be explored to provide a similar interruption method for the flyer material in a solid-state slapper detonator. The following list offers some recommendations for future work in developing a MEMS-based interrupter mechanism for state-of-the-art safe and arm devices.

- Optimize deflection by using an alternative actuation method. For example, a ratcheting mechanism could be created with the bent-beam, or u-shaped, electrothermal actuators that could dramatically increase the distance over which the interrupter plates could move. This increased movement would result in a far greater aperture area.
- Design a gear system operated by scratch drives that is capable of moving a single interrupter plate in-line to pass the flyer material, and out-of-line to prevent the flyer material from initiating the HE pellet. Multiple scratch drives could be implemented so that the interrupter plate can move in both directions.
- Investigate using bent-beam actuators with less than 8 arms to further reduce power consumption. Note the resulting reduction in force should not be an issue based on the required force calculations performed as part of this thesis.
- Implement an operational latching mechanism, possibly based on the 3 4 μm width suggested in Chapter 5. This latching mechanism could include an unlatching capability that would enable the S&A interrupter device to return to the safe mode after having received an arming signal.

- Redesign the current interrupter mechanism to optimize the components for a more efficient use of chip area. Sinclair et al. offers some suggestions using a *folded* bent-beam electrothermal actuator design [8].
- Etch through a MUMPs® die, under the interrupter plates, to determine if an adequate hole could be created in the substrate that would allow for the flyer material to pass through when the interrupter plates are in the open (armed) position.
- Investigate wafer bonding of the die containing the interrupter mechanism to another die that functions as the barrel in a solid-state slapper detonator.
- Design and fabricate an alternative interrupter scheme where an out-of-line barrel plate functions as the interrupter for the flyer material, and is physically moved in-line when armed [9].
- Design and fabricate an alternative MEMS safe and arm mechanism that keeps a micro-scale HE pellet normally out-of-line (safe), then physically moves the HE pellet in-line when armed [10].
- Fabricate a solid-state slapper detonator, or components thereof, i.e., fabricating a solid-state capacitor capable of being charged to multi-kilovolt potentials and delivering large current pulses [10].

Bibliography

- [1] Skibbie, Lawrence F. "Fuze Industrial Base Problems Should No Longer Be Ignored," *National Defense Magazine*, (June 2001). March 2005. http://www.nationaldefensemagazine.org/issues/2001/Jun/Fuze Industrial.htm.
- [2] Erwin, Sandra I. "Army Not Producing Enough Ammunition," *National Defense Magazine*, (May 2003). June 2005. http://www.nationaldefensemagazine.org/ issues/2001/Dec/Munitions Sector.htm>.
- [3] Erwin, Sandra I. "Munitions Sector 'In Trouble,' Despite New Funds," *National Defense Magazine*, (December 2001). June 2005. http://www.nationaldefensemagazine.org/issues/2001/Dec/Munitions Sector.htm>.
- [4] Koester, David and others. *PolyMUMPs Design Handbook (Revision 11.0)*. MEMSCAP, 2005. August 2005. http://www.memsrus.com/documents/PolyMUMPs.DR.v11.pdf.
- [5] Cowan, Allen and others. *MetalMUMPs Design Handbook (Revision 1.0)*. MEMSCAP, 2002. January 2005. http://www.memsrus.com/documents/MetalMUMPs.dr.v1.pdf>.
- [6] Kovacs, Gregory T. A. *Micromachined Transducers Sourcebook*. Boston: The McGraw Hill Company, 1998.
- [7] Sharpe Jr., W. N., K. Jackson, G. Coles, and D. A. LaVan. "Young's Modulus and Fracture Strength of Three Polysilicons," *Proceedings of Materials Science of Microelectromechanical Systems (MEMS) Devices III.* Volume 657: 551-556. Materials Research Society, 2001.
- [8] Sinclair, Michael J. and Kerwin Wang. "Thermal Actuator Improvements: Tapering and Folding," *Proceedings of the SPIE The International Society for Optical Engineering*. Volume 5116: 237-251 (April 2003).
- [9] Garvick, Donald R., Lawrence C. Fan, Bruce R. Kuester, and Gregory R. Birk. "MEMS Energetic Actuator with Integrated Safety and Arming System for a Slapper/EFI Detonator." US Patent 6173650. 16 January 2001.
- [10] O'Brien, Dennis W., Robert L. Druce, Gary W. Johnson, George E. Vogtlin, Troy W. Barbee Jr., and Ronald S. Lee. "Method and System for Making Integrated Solid-State Fire-Sets and Detonators." US Patent 5731538. 24 March 1998.

Appendix A.Release Procedures for Microelectromechanical Systems

The specific release procedures used for the devices produced for this research effort are described in the following paragraphs. The chemicals used were acetone, methanol, deionized water (DIW), and a 48% hydrofluoric acid (HF) solution. Several variations of these release procedures were attempted in the beginning of this effort and the following method was finally adopted because it consistently produced the best results. The criteria used to determine the best results were completely released structures (i.e., no oxide remained beneath the structures) and cleanliness of the entire die. In some early variations of the release procedures, particulates were observed on the surface of the dies that could potentially prevent successful device operation. It was hypothesized that these particulates most likely came from remnants of silicon dust that comes from dicing and the protective photoresist removed by the acetone. Therefore, the immersion in a single acetone bath was split into two separate acetone baths.

Another modification to the early release procedures was the die immersion time in the HF solution. The general release instructions provided by the MUMPs[®] website states that a 2-2.5 min. immersion in an HF bath should completely free the structures from the sacrificial oxide layers [1]. However, it must be noted that for devices with dimensions greater than 50 μ m, etch holes should be fabricated in the structural material to allow the HF to access the oxide [2]. Therefore, with these recommendations in mind, etch holes were fabricated on the two releasable polysilicon layers and an HF immersion time of 4.0 min. was used to ensure a successful release. The complete procedures are listed in Appendix A, along with the main purpose for including that step in the process.

Table A-1. Release procedures used for MEMS dies fabricated in this research effort.

Step	Chemical	Time	Main Purpose
1	Acetone	10 min	Removes the protective photoresist layer.
2	Acetone	10 min	Clears the particulates removed from the previous step and continues to remove the protective photoresist.
3	Methanol	5 min	Rinses the acetone from the die and clears any particulates remaining from the previous step.
4	DIW	2 min	Rinses the methanol from the previous step. (This time is flexible)
5	48% HF	4 min	Etches the sacrificial oxide layer from between the two structural polysilicon layers.
6	DIW	10 sec	Stops the HF etching process.
7	Methanol	2 min	Rinses the DIW from the previous step and prepares the dies for the supercritical CO ₂ drying process.

The supercritical drying method was used exclusively for removing the methanol from the dies. The main purpose of the supercritical CO₂ drying procedure is to completely avoid the surface tension effects that often lead to stiction in MEMS structures. Stiction is a leading cause of low yield in MEMS fabrication, and reducing its occurrences can increase manufacturing efficiencies. Surface tension arises in the drying process when liquid CO₂ transitions to CO₂ vapor. This interface point can be circumvented by cycling through a specific sequence of pressure and temperature changes that result in the liquid CO₂ transitioning directly to vapor form [3]. Figure depicts the cycle required for supercritical drying on a CO₂ phase diagram and a summary of the process is described in the following paragraph.

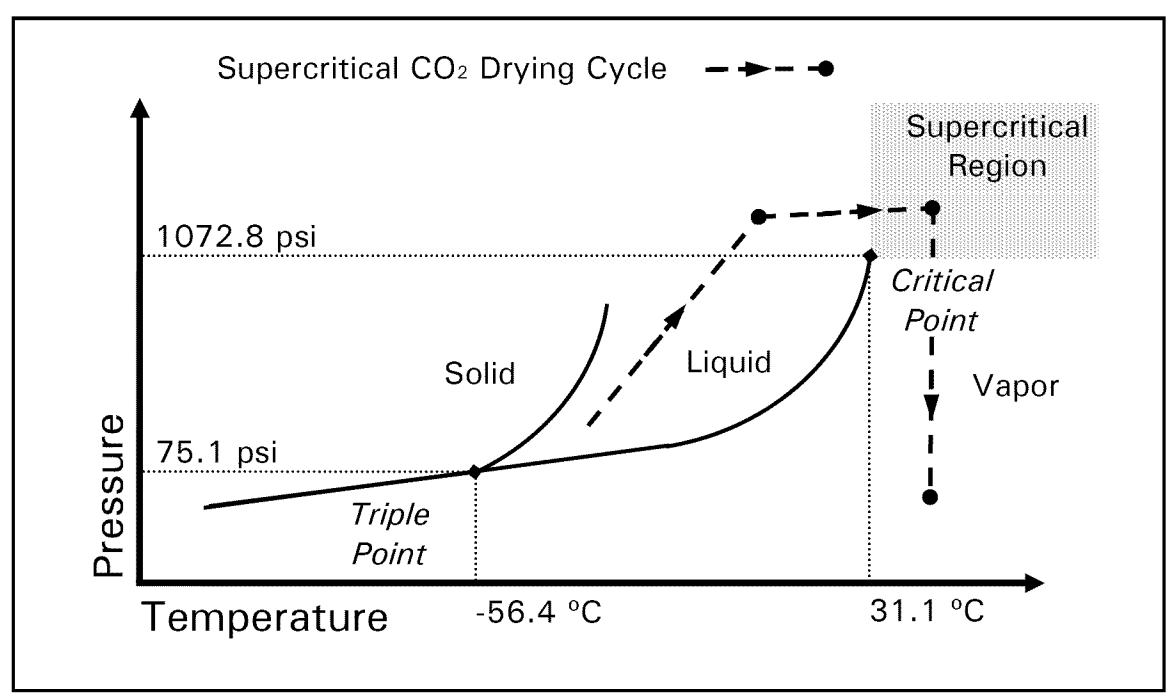


Figure A-1. Carbon dioxide phase diagram showing the supercritical CO₂ drying cycle.

The specific equipment used for this process was an Autosamdri®-815, Series B Automatic Supercritical Point Dryer as shown in Figure A-2. The MEMS dies are placed into the methanol-filled chamber of the supercritical CO₂ dryer at room temperature. Next, the chamber is cooled and purged with liquid CO₂ to replace the methanol. The pressure of the chamber is then raised to above 1072.8 psi (the model used here stabilized at approximately 1350 psi), while the temperature is increased to just above 31.1 °C. At this point, the pressure and temperature is above the critical point for CO₂ and the liquid transitions directly into the vapor phase through the supercritical region. Finally, the CO₂ gas is vented from the chamber at a constant temperature [3], [4]. This procedure proved very effective for drying MEMS devices without inducing stiction damage.

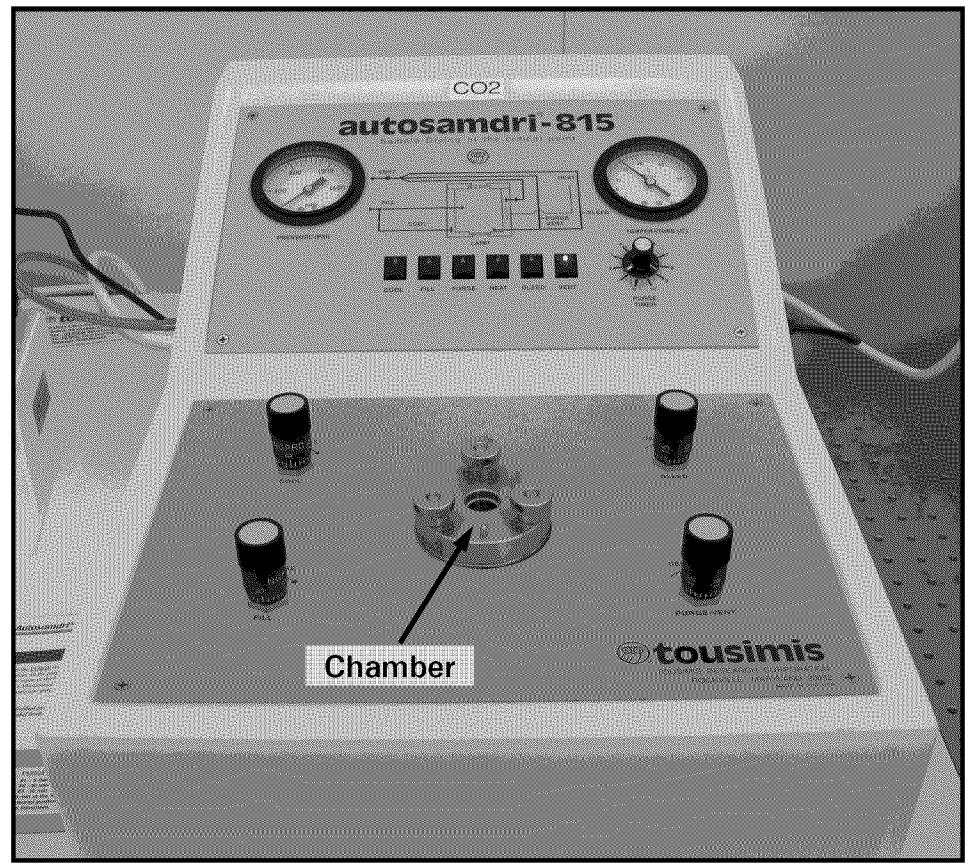


Figure A-2. Automatic supercritical CO₂ dryer used to prevent stiction in the MEMS dies used in this research effort.

- [1] "PolyMUMPs[™] General Release Instructions." *PolyMUMPs Reference Library*. Durham: MEMSCAP. January 2006. http://www.memsrus.com/documents/PolyMUMPs.Release.Instructions.pdf>.
- [2] *PolyMUMPs FAQ (Revision 2.0)*. MEMSCAP, 2004. August 2005. http://www.memsrus.com/documents/PolyMUMPs.faq.v2.pdf>.
- [3] Jafri, Ijaz, Heinz Busta, and Steven Walsh. "Critical Point Drying and Cleaning for MEMS Technology," Proceedings of SPIE The International Society for Optical Engineering. Volume 3880: 51-58 (September 1999).
- [4] Autosamdri®-815, Series B User Manual. Serial Number 2112. Rockville: Tousimis, 2003.